

Polarized Raman Spectroscopy to Elucidate the Texture of Synthesized MoS₂

Received 00th January 20xx,
Accepted 00th January 20xx

Vincent Vandalon*, Akhil Sharma, Alberto Perrotta, Benedikt Schrode, Marcel A. Verheijen, Ageeth A. Bol

DOI: 10.1039/x0xx00000x

Impact of strain and grain size on the Raman response

The impact of texture on the Raman response of nanocrystalline TMDs as shown in this work should be placed in the context of other phenomena that are likely to occur in these films that affect the Raman response. An overview of the most likely phenomena impacting the A_{1g}/E_{2g} ratio will be given based upon a literature study. With this overview, it is then possible to determine the significance of changes in the A_{1g}/E_{2g} ratio caused by texture or whether texture effects could be masked by other phenomena. The most likely phenomena relevant for these nanocrystalline films are strain, defects, grain size, and the thickness (*i.e.* the number of layers). These phenomena are known to impact the Raman response, manifesting itself as changes in peak position and peak broadening but also as changes in peak intensity and, as such, affect the peak ratios. For single crystalline MoS₂ these effects have already been investigated in detail but these studies have mainly focused on changes in the peak width and peak position. Nevertheless, these studies can be used as a starting point to judge the extent of the impact of strain, defects, and thickness on the A_{1g}/E_{2g} ratio by re-analyzing the data published in this context.

The influence of strain on the Raman response of MoS₂ was studied by Wang *et al.*¹ They placed a monolayer of MoS₂, obtained by exfoliation, on a PET substrate. The Raman response of the MoS₂ was measured without applying external strain and after applying 1% and 2% uniaxial strain on the PET, see also Fig.S1. Apart from a shift in the A_{1g} and E_{2g} peak position, also a change in the A_{1g}/E_{2g} ratio from 1.3 to 1.2 under the 2% strain was observed. Although this change in the A_{1g}/E_{2g} ratio is relevant, it should be noted that a 2% strain can be realized in a single crystal but is less likely that a grain in a nanocrystalline film experiences the stress associated with such a strain.

The influence of the number of MoS₂ layers was studied by Lee *et al.*² They reported on the peak position, peak width, and A_{1g}/E_{2g} ratio as a function of stacked MoS₂ layers ranging from 1 up to 6 and a bulk MoS₂ film. They found that a A_{1g}/E_{2g} ratio of 0.77 for

all but the monolayer cases which showed a A_{1g}/E_{2g} ratio of 1.05.² A similar trend was reported by Li *et al.*³ but in both cases, no explanation of this atypical behavior was given.

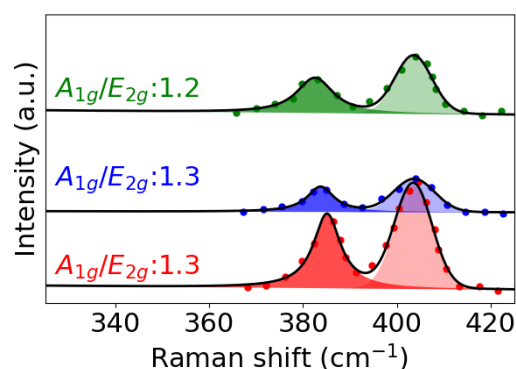


Figure S1. Raman response of exfoliated MoS₂ placed on a PET substrate without external strain (lower spectrum) and under 1% and 2% external uniaxial strain (middle and upper spectrum, respectively) taken from Wang *et al.*¹ The A_{1g}/E_{2g} ratio was obtained from a fit to the data (solid lines). Data reproduced with permission of John Wiley and Sons.

The impact of the defect and defect density on the Raman response of MoS₂ was studied by Mignuzzi *et al.*,⁴ mainly focusing on the appearance of new peaks (caused by symmetry breaking due to defects) and studying line width and frequency shifts. In their work, an exfoliated monolayer of MoS₂ was bombarded by Mn⁺ atoms yielding a tunable and controllable defect distance ranging from 10 nm down to 1 nm depending on the ion dose. The Raman spectra reported by Mignuzzi *et al.* show a significant peak broadening together with virtually no peak shift for the A_{1g} and E_{2g} contributions as a function of increasing defect density, as shown in Fig. S2.⁴ Furthermore, they identified several Brillouin zone-edge modes related to defects such as the LA(M) peak at 227 cm⁻¹.⁴ However, their work can also be used to gauge the impact of defects on the A_{1g}/E_{2g} ratio. The A_{1g}/E_{2g} ratio extracted from the fit to the data in Fig. S2 shows that the peak ratio varied from 1.6 down to 0.7 for heavily damaged MoS₂. This is in a large part due to the appearance of transverse optical (TO), longitudinal optical (LO), and out-of-plane optical (ZO) phonons originating from the M point of the Brillouin zone.² Also a spectrally isolated defect-allowed LA(M) peak appears at 227 cm⁻¹ which is well

suited as a measure of the (relative) defect density.² These modes originating from the M point in the Brillouin zone are forbidden in pristine material by momentum conservation and only appear in the presence of defects due to the more relaxed selection rules. It is not straightforward to isolate the A_{1g} and the E_{2g} contributions from the overlapping zone-edge optical contributions. Therefore, the interpretation of the intensity and area of the A_{1g} and to a lesser extent the E_{2g} is difficult for (highly) defective material. The two Raman spectra shown in Fig. S2 of the damaged material represent a more extreme situation than encountered in practice for synthesized material judging from the broadening of the A_{1g} peak caused by the zone-edge optical modes.

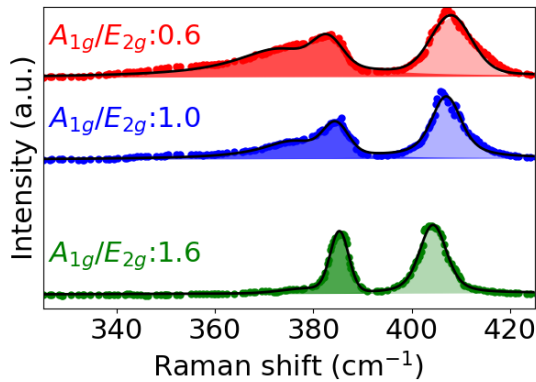


Figure S2. Raman spectra taken from Mignuzzi et al. (markers) of exfoliated MoS₂.⁴ The pristine material (bottom spectrum) was exposed to increasing ion implantation doses (upwards), resulting in a defect density of 7 nm and 3 nm, respectively. To determine the A_{1g}/E_{2g} ratio, as indicated in the figure, the spectra were fitted (solid lines) from which the ratio was determined. Data reproduced with permission of American Physical Society.

The impact of defect distance, layer thickness, and strain likely to occur in synthesized nanocrystalline MoS₂ on the A_{1g}/E_{2g} ratio is relatively small compared to the impact of texture reported in this work. The modeling of the various textures predicted a change of the A_{1g}/E_{2g} ratio by a factor of ~ 2 going from in-plane to out-of-plane oriented material. Similarly, the experimental results show an equally large variation in the A_{1g}/E_{2g} for films synthesized with different textures. Therefore, if texture is varying between samples, this should be considered as one of the main factors causing differences in the A_{1g}/E_{2g} ratio in the Raman spectra.

Impact instrumental sensitivity on A_{1g}/E_{2g} ratio in unpolarized Raman spectroscopy

In contrast to the polarized Raman, the A_{1g}/E_{2g} ratio measured using a non-polarized Raman set-up is impacted by the sensitivity of the instrument to s and p polarized light. The A_{1g} and E_{2g} contributions emit light with different polarization (linear and elliptical,

respectively) and therefore the A_{1g}/E_{2g} ratio will be affected by the difference in sensitivity. This results in a large spread of A_{1g}/E_{2g} ratios reported for MoS₂ in literature, as summarized in Tab. S1. Typically, the main source of this variation in sensitivity is the grating used in the experiment. For example, an efficiency of 75% for s and 45% for p is quite typical for the high l/mm gratings blazed for e.g. 600 nm used in these measurements (larger mismatches are inherent to multi wavelength systems) skewing the ratio by as much as a factor $\frac{0.45}{0.45+0.74} = 0.375$ from the ideal measurement. For the polarized measurements, only 1 polarization state is measured at a time and the grating efficiency for that particular polarization state on the A_{1g}/E_{2g} ratio is divided out. To summarize, A_{1g}/E_{2g} ratios obtained in a non-polarized setup should not be interpreted quantitatively nor should results from different setups be compared.

Other factors influencing the A_{1g}/E_{2g} ratio, although to a lesser extent, are the choice in NA of the microscope objective and excitation wavelength, see also Table S1. The impact of the NA will be treated later and the excitation wavelength only plays an important role when the excitation energy matches an electronic transition in the materials, such as is the case for WS₂ using a 532 nm laser.^{5,6}

Evaluation of the Raman model and analytical results of Equation (2)

To calculate the Raman response for each of the Raman modes as described by Eq. (2), several steps have to be taken. First, the Raman tensors of the vibrations of interest have to be known. For the 2D TMDs with the D_{3h}/D_{6h} symmetry, the tensors have the following shape:

$$\begin{aligned} A_{1g} &= \begin{pmatrix} a & 0 & 0 \\ 0 & a & 0 \\ 0 & 0 & b \end{pmatrix} \\ E_{2gx} &= \begin{pmatrix} c & 0 & 0 \\ 0 & -c & d \\ 0 & d & 0 \end{pmatrix} \\ E_{2gy} &= \begin{pmatrix} 0 & -c & -d \\ -c & 0 & 0 \\ -d & d & 0 \end{pmatrix} \end{aligned} \quad (S1)$$

where the $a, b, c,$ and d coefficients are unique for each TMD and the numerical value can be determined by the procedure described in the next section. Also, a description of the electric field exciting the material, E_{in} and the collection of the scatter light given by E_{out} is needed which are taken from Turrel *et al.* and Boivin and Wolf.⁷⁻⁹ The excitation light can be described by:

$$\vec{E}_{in}(u, v, \psi) = \begin{bmatrix} -i(I_0(u, v) + I_1(u, v)) \cos(2\psi) \\ -iI_2(u, v) \sin(2\psi) \\ 2I_1(u, v) \sin(\psi) \end{bmatrix} \quad (\text{S2})$$

Table S1. An overview of the key parameters of the Raman set-up used in the cited publications. The p/s ratio was calculated from the area of the A_{1g} peak of c-cut sapphire measured without a polarizer for p and s polarized input light. The largest impact on the A_{1g}/E_{2g} ratio is most likely caused by the grating, followed by the NA of the microscope objective. Unfortunately, most works do not specify sufficient information to judge the impact of the grating.

	Unpolarized A_{1g}/E_{2g} ratio	Grating (l/mm)	Measured p/s ratio	NA	Excitation λ (nm)
This work	1.7	1800	1.46	0.75	532
Mignuzzi <i>et al.</i> ⁴	1.6	600	-	0.9	532
Lee <i>et al.</i> ²	1.3	Not reported	-	40x (likely NA=0.65)	514.5 & 532
Wang <i>et al.</i> ¹	1.1	1800 & 150	-	0.95	532

with the I_x terms as defined in Boivin and Wolf which are integral of Bessel functions.⁷⁻⁹ The collected of the scattered light given by,⁷⁻⁹

$$\vec{E}_{out}(\theta', \phi', \psi') = \begin{bmatrix} -\cos(\theta') \cos(\phi') \sin(\psi') - \sin(\phi') \cos(\psi') \\ -\cos(\theta') \sin(\phi') \sin(\psi') + \cos(\phi') \cos(\psi') \\ \sin(\theta') \sin(\psi') \end{bmatrix} \quad (\text{S3})$$

With these definitions, Eq. (2) can be reduced (especially making use of the symmetry of the electric fields) to the following equation:

$$\begin{aligned} I &= A_{xx}(B_{xx} \iiint \hat{\chi}_{xx}^2 + B_{yy} \iiint \hat{\chi}_{yy}^2 + B_{zz} \iiint \hat{\chi}_{zz}^2) \\ &+ A_{yy}(B_{xx} \iiint \hat{\chi}_{yx}^2 + B_{yy} \iiint \hat{\chi}_{yy}^2 + B_{zz} \iiint \hat{\chi}_{yz}^2) \\ &+ A_{zz}(B_{xx} \iiint \hat{\chi}_{zx}^2 + B_{yy} \iiint \hat{\chi}_{zy}^2 + B_{zz} \iiint \hat{\chi}_{zz}^2) \end{aligned} \quad (\text{S4})$$

with the integral variables $d\theta''$, $d\psi''$, $d\phi''$ omitted in each of the integrals for brevity, and A defined as,

$$A_{ij} = \iiint d\theta' d\psi' d\phi' \sin(\theta') E_{out}^i E_{out}^j = -1/3\pi^2 \begin{cases} (-4 + 3 \cos(\theta_m) + \cos(\theta_m)^3) & i = j = x \\ (-4 + 3 \cos(\theta_m) + \cos(\theta_m)^3) & i = j = y \\ -1/2(8 - 9 \cos(\theta_m) + \cos(3\theta_m)) & i = j = z \\ 0 & i \neq j \end{cases} \quad (\text{S5})$$

and B defined as,

$$B_{ij} = \iiint v dudv \int |E_{in,i}|^2 d\psi = \iiint dudv v \begin{cases} \pi(2|I_0|^2 + |I_2|^2) & i = j = x \\ \pi|I_2|^2 & i = j = y \\ 4\pi|I_1|^2 & i = j = z \\ 0 & i \neq j \end{cases} \quad (\text{S6})$$

In the last equation (eq. S6), I_0 , I_1 , and I_2 are solely a function of the NA of the objective, see Boivin and

Wolf.⁷ The triple integral in Eq. (S4) is applied to each element of the Raman tensor using $\hat{\chi}_{ij}^2 = W(\theta') |\Phi R_x{}_{ij} \hat{\Phi}|^2$. Basically, a new “squared” Raman tensor can be introduced which account for the angular grain distribution and is calculated by evaluating these integrals element wise. For the A_{1g} mode assuming the uniform distribution, this results in:

$$(A_{1g})_{uni}^2 = \begin{pmatrix} \frac{1}{8} (41a^2 + 14ba + 9b^2) \pi^3 & \frac{3}{8} (a-b)^2 \pi^3 & \frac{1}{2} (a-b)^2 \pi^3 \\ \frac{3}{8} (a-b)^2 \pi^3 & \frac{1}{8} (41a^2 + 14ba + 9b^2) \pi^3 & \frac{1}{2} (a-b)^2 \pi^3 \\ \frac{1}{2} (a-b)^2 \pi^3 & \frac{1}{2} (a-b)^2 \pi^3 & (3a^2 + 2ba + 3b^2) \pi^3 \end{pmatrix} \quad (\text{S7})$$

The intensity can now be expressed in the parameters of the chosen distribution together with the A and B parameters associated with the NA of the objective of interest. To reduce the length of the expression, the numerical values for the A and B terms were used, assuming an NA=0.75, resulting in an intensity for the A_{1g} mode in the parallel configuration of:

$$I_{A1g} = 1619a^2 + 426ab + 418b^2 \quad (\text{S8})$$

And for the cross polarized configuration this results in:

$$I_{A1g} = 195a^2 + 323ab + 193b^2 \quad (\text{S9})$$

Note that the E_{2g} mode is omitted for brevity and hence the c and d coefficient do not appear in these equations. For the more complex Gaussian and delta distribution, the tensors become lengthy, but it is still an analytical expression of the parameters describing the distribution. This analytical nature is also reflected in the expression for the intensity, again

making use of the numeric values of the A and B terms to reduce the length of the expression. The intensity of the A_{1g} mode for the Delta distribution in the parallel configuration is given by:

$$I_{A_{1g}} = 257a^2 + 67ab + 66b^2 + (114a^2 + 47ab - 66b^2) \cos(2\theta_p) + (10a^2 + 20ab + 10b^2) \cos(4\theta_p). \quad (S10)$$

It is worth noting that this equation does indeed still explicitly contains the predominant angle, θ_p . And for the cross polarized configuration:

$$I_{A_{1g}} = 31a^2 - 51 + 30b^2 + (-28a^2 + 47ab - 19b^2) \cos(2\theta_p) + (-1a^2 + 3ab - 2b^2) \cos(4\theta_p) \quad (S11)$$

It turns out for a generic tensor (i.e. all elements unique and non-zero), the analysis is the same and that it is still possible to find a closed analytical expression for the Raman intensity for the uniform, Gaussian, and delta distribution. Therefore, for a Raman tensor of interest, the appropriate coefficients can be set and the result for the specific angular grain distributions is known. For example, nanocrystalline Indium Oxide, with cubic space group Ia-3, can therefore also be modelled with the approach presented in this work. The generic result is made available as a *Mathematica* © file.

Determining tensor elements of MoS_2

In order to evaluate the Raman response of nanocrystalline material with the model introduced in this paper, the numerical value of the elements of Raman tensors of the A_{1g} and E_{2g} mode need to be known for the specific TMD. For some common materials such as c-Si the numerical values of the tensor elements can be found in literature, but even for the well-studied case of MoS_2 this information was not available to our knowledge. Therefore the tensor elements needed to be determined from a series of reference measurements for a sample with known texture. A thick exfoliated flake of MoS_2 was used as the reference sample and its polarized Raman response was measured. MoS_2 powder was also considered as a possible reference sample, however, due to scattering (e.g. partial depolarization) of the laser light on the powder itself, the polarization state is unclear, making this a less ideal reference sample. The Raman response for the two polarization configuration can be written as a function depending

solely on the 4 tensor elements for a specific texture using the derived model. This means that the tensor elements can be found by fitting the model - using the tensor elements as fit parameters - to either (1) the measured peak areas, or (2) the measured A_{1g}/E_{2g} ratios. At first glance the A_{1g}/E_{2g} strategy seems superior because the impact of a possible variations in probing power are suppressed. However, the best strategy was found by considering the partial derivative of the fitted quantity (either peak intensity or A_{1g}/E_{2g} ratio) with respect to the tensor elements. These partial derivatives are a measure for the sensitivity of the procedure to each of the tensor elements. Using the peak area showed a roughly equal sensitivity for all the tensor elements, whereas, using the two A_{1g}/E_{2g} ratios showed negligible sensitivity to the d tensor element. Therefore, the peak area was used to determine the tensor elements, resulting in: $a = 195, b = 276, c = 125, d = 0$. It turns out that the d tensor element is small compared to the other tensor elements of MoS_2 but this might be different for other TMDs. This procedure yields the relative value of the tensor elements (not corrected for input and output power) and therefore the elements are taken to be dimensionless.

Impact NA on Raman Mappings of the A_{1g}/E_{2g} ratios

With the Raman model it is possible to evaluate the impact of the NA used in the experiment on the Raman response. Figure S3 shows the A_{1g}/E_{2g} ratio for two different NAs, where especially the cross polarized mappings shows a large differences with NA. For a high NA=0.9, a larger and more constant A_{1g}/E_{2g} ratio is predicted for the cross polarized mode than the result for a NA=0.75 (see Fig. 4) and NA=0.5. This effect can also be understood: The z-component of the electric field driving the Raman process becomes larger for higher NA. This especially impacts the cross polarized mode, where the z-component causes a significant A_{1g} signal even for the in-plane materials ($\theta_p = 0$ and $\alpha \rightarrow 0$). Furthermore, because the strength of the electric field in all directions becomes more equal in the high NA case - probing the material more isotropically - the orientation of the grains becomes less relevant resulting in less variation in the A_{1g}/E_{2g} ratio.

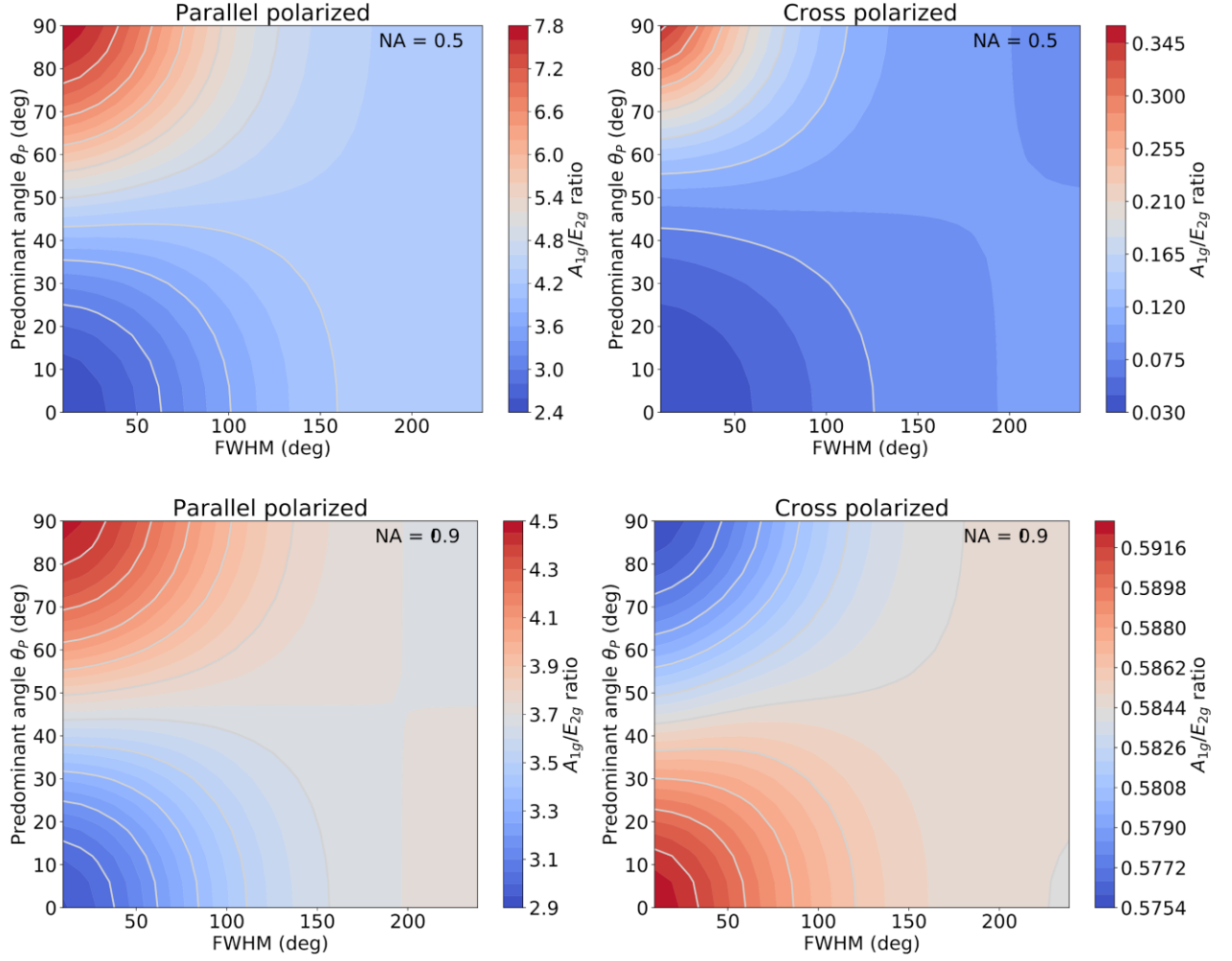


Figure S3. The mapping of the A_{1g}/E_{2g} ratio for MoS_2 when probed with a microscope objective with a NA of 0.9 (upper) and 0.5 (lower). The differences between the two mappings are solely due to the difference in NA and the same tensor elements have been used in the evaluation. Note the compressed scale for the NA=0.9 for the cross polarized configuration.

Fourier analysis of grain orientation in cross-section TEM data

A cross-section TEM image can be used to get an indication of the approximate shape of the angular grain distribution. In a cross-section TEM image, the dissected 2D layers can easily be identified from their well-known lattice spacing (c) and the orientation of the layers is also apparent from the image. In Fourier space, all the grains lie on a ring at $1/c$ from the origin, with the intensity at a specific angle representative of the fraction of material with that specific orientation. Figure S3 shows the 2D Fourier transform of the image in Fig. 5, clearly showing a weak ring dominated by four spots. A measure for fraction of material with the c -axis making a θ angle with the horizontal, $W_{TEM}(\theta)$, can now be calculated by integrating the total intensity in the annulus sector with an angle between $\theta - \delta$ and $\theta + \delta$ and with a

radius between $\frac{1}{c} - \delta$ and $\frac{1}{c} + \delta$. The result is the angular grain distribution $W_{TEM}(\theta)$ that is shown in Fig. 5.

The fidelity of the angular grain distribution determined from the cross-section TEM image is mainly limited by two effects: (1) All dissected in-plane material will appear in the TEM cross section as a 2D layer, whereas, only a fraction of the dissected out-of-plane material will appear as 2D layers in the TEM cross section. To appear in the TEM image as a 2D layer, the c -axis has to be perpendicular to the electron beam. In-plane material will always have its c -axis perpendicular to the electron beam irrespective of a rotation around the surface normal. For out-of-plane material, a rotation around the surface normal will impact the angle between the electron beam and the c -axis and only at specific orientations will a grain appear as a 2D layer. (2) The field-of-view of a single TEM image is too narrow to get a reliable angular grain distributions from a single

image. Therefore, the angular grain distribution determined from the TEM image should not be expected to be representative of the angular grain distribution probed by *e.g.* XRD or polarized Raman. Nevertheless, the angular grain distribution determined from a cross-section TEM image can give qualitative insight into the *actual* angular grain distribution.

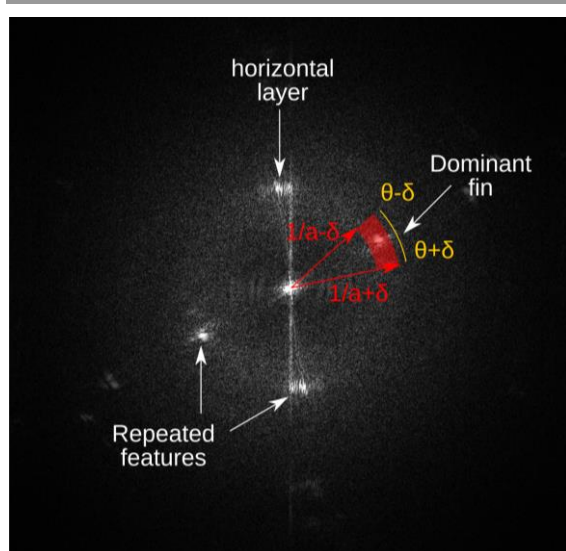


Figure S4. The 2D Fourier transform of the cross-section TEM image in the paper. The annulus sector used for integration that is rotated over the image is also shown. The dimensions are exaggerated for illustration purposes and the symmetry related annulus sector rotated by π radians is omitted

the MoS₂ film is probed showing predominantly OoPO material, *i.e.* 100 texture, whereas at an angle of 1° the full film is measured showing both OoPO and in-plane material. This procedure was repeated for the MoS₂ film grown by 200 cycles and the resulting angular grain distribution is shown in Fig. 7 in the main text. To determine the OoPO fraction, the area under the curve in Fig. 7 (b) was determined using the inflection point of the curve as the demarcation between in-plane oriented and OoPO material.

Texture analysis of 2D GIXD measurements

2D GIXD patterns of the MoS₂ films grown by 200 and 500 cycles of ALD were recorded at two angles of incidence (0.2° and 1.0°). The complementary 2D GIXD pattern measured at 0.2° is shown in Fig. S5 complementary to the pattern shown in Fig. 7 of the main text which was recorded at an angle of incidence of 1.0°. Pole figures of the 002 reflection were constructed from these 2D GIXD pattern recorded at 180 different phi angles (rotation of sample around the surface normal) with the aid of *GIDVis*,¹⁰ a software package taking *e.g.* polarization and space-angle effects into account. The resulting pole figure for the 0.2° angle of incidence is also shown in Fig. S5. The pole figures for both samples show no intensity variation as a function of phi, in-line with the expected fibre texture. This allows a simplified representation of the angular grain distribution (or ODF) plotting the intensity of the 002 reflection as a function of psi (the angle between the surface normal and the c-axis of the MoS₂ unit cell). Figure S5 also shows the resulting angular grain distribution measured for the two different angle of incidence. At an angle of 0.2° only the upper part of

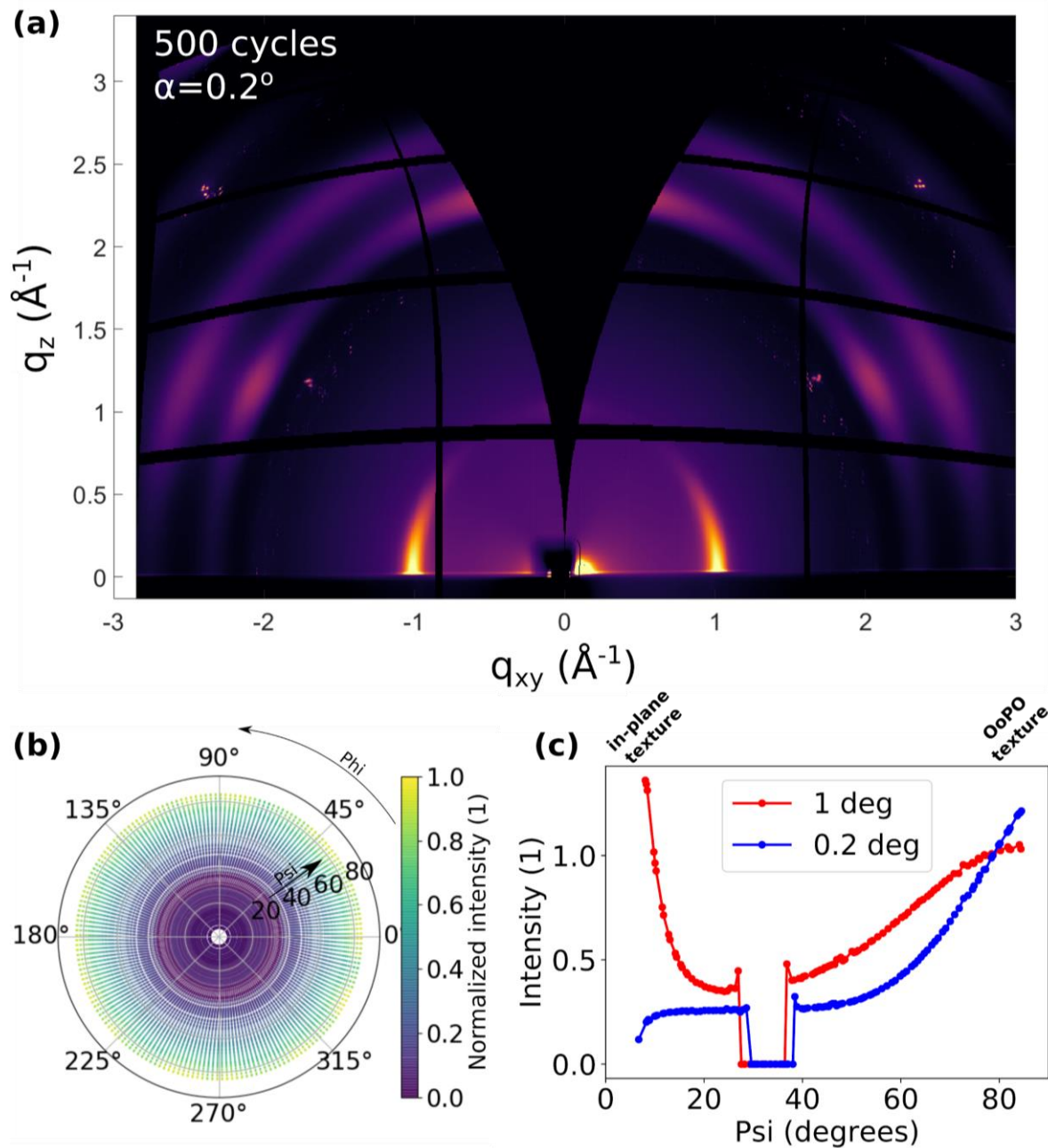


Figure S5. (a) 2D GIXD data measured with an incident angle α of 0.2° summed over all recorded ϕ angles of the MoS₂ film grown by 500 ALD cycles. (b) The pole figure calculated from the individual 2D GIXD patterns recorded at α of 1° of the 500 cycle thick sample using GIDVis. (c) The GIXD intensity of the 002 reflection calculated from a pole plot composed of 180 2D GIXD spectra measured on a 500 cycles thick PE-ALD grown MoS₂ film comparing the data measured at 1° and 0.2° angle of incidence.

References

- 1 Wang, Y., Cong, C., Qiu, C. & Yu, T. Raman spectroscopy study of lattice vibration and crystallographic orientation of monolayer MoS₂ under uniaxial strain. *Small* **9**, 2857–2861 (2013).
- 2 Lee, C. *et al.* Anomalous lattice vibrations of single- and few-layer MoS₂. *ACS Nano* **4**, 2695–2700 (2010).

- 3 Li, H. *et al.* From bulk to monolayer MoS₂: Evolution of Raman scattering. *Adv. Funct. Mater.* **22**, 1385–1390 (2012).
- 4 Mignuzzi, S. *et al.* Effect of disorder on Raman scattering of single-layer MoS₂. *Phys. Rev. B* **91**, 1–7 (2015).
- 5 Groven, B. *et al.* Plasma-Enhanced Atomic Layer Deposition of Two-Dimensional WS₂ from WF₆, H₂ Plasma, and H₂ S. *Chem. Mater.* acs.chemmater.6b05214 (2017).
- 6 Weber & Merlin. *Raman Scattering in Materials Science*. (Springer-verlag Berlin Heidelberg, 2000).

- 7 Boivin, A. & Wolf, E. Electromagnetic Field in the Neighborhood of the Focus of a Coherent Beam. *Physical Review* **138**, B1561–B1565 (1965).
- 8 Bremard, C., Dhamelincourt, P., Laureyns, J. & Turrell, G. Effect of High-Numerical-Aperture Objectives on Polarization Measurements in Micro-Raman Spectrometry. *Appl. Spectrosc.* **39**, 1036–1039 (1985).
- 9 Turrell, G. Analysis of polarization measurements in Raman microspectroscopy. *J. Raman Spectrosc.* **15**, 103–108 (1984).
- 10 B. Schrode, S. Pachmajer, M. Dohr, C. Röthel, J. Domke, T. Fritz, R. Resel, and O. Werzer. GIDVis – a Comprehensive Software Tool for Geometry-Independent Grazing-Incidence X-Ray Diffraction Data Analysis and Pole-Figure Calculations. *J. Appl. Crystallogr.* **52**, (2019).